Accurate State of Charge Estimation With Model Mismatch for Li-Ion Batteries: A Joint Moving Horizon Estimation Approach

Jia-Ni Shen, Jia-Jin Shen, Yi-Jun He, and Zi-Feng Ma

***Abstract*—The accurate state of charge (SOC) estimation plays a significant role in charge/discharge control, balance control, and safe management of lithium-ion batteries (LIBs). However, due to the model mismatch issues, either from battery inconsistency or battery dynamic characteristics difference, the accuracy of the model-based SOC estimation method is usually unsatisfactory. To solve this problem, a joint moving horizon estimation (joint-MHE) approach that can simultaneously estimate the model parameter and state is proposed here. In this paper, the circuit-equivalent battery model is first constructed by parameterizing the circuit parameters as polynomial function of SOC. Then, by the sensitivity analysis, the update parameters are selected and added to the state-space model as additional states. Finally, the joint-MHE strategy is conducted for the simultaneous parameter and SOC estimation. To investigate the performance of the proposed method thoroughly, three model mismatch conditions are considered, including battery inconsistency, battery dynamic characteristics difference, and the combination of both. The results demonstrate that the joint-MHE approach is an effective way to solve the model mismatch problem. Moreover, compared to joint extended Kalman filtering, the proposed approach can offer a more reliable, robust, and accurate SOC estimation of LIBs under various model mismatch conditions.**

***Index Terms*—Equivalent circuit model (ECM), joint moving horizon estimation (joint-MHE), lithium-ion batteries (LIBs), model mismatch, state of charge (SOC).**

I. Introduction

ALTHOUGH lithium-ion batteries (LIBs) powered electric vehicles have experienced rapid development in recent years, the increasing number of battery-related failures and accidents indicates that the efficient and safe usage of LIBs still faces a great challenge [1], [2]. Therefore, the advanced battery management system (BMS) that can provide the safe and reliable operation of LIBs attracts more and more attention. A typical

Manuscript received January 24, 2018; revised April 16, 2018 and June 10, 2018; accepted July 17, 2018. Date of publication August 2, 2018; date of current version March 29, 2019. This work was supported by the National Key R&D Program of China under Grant 2016YFB0901500. Recommended for publication by Associate Editor Y.-M. Chen. *(Corresponding author: Yi-Jun He.)*

J.-N. Shen, Y.-J. He, and Z.-F. Ma are with the Department of Chemical Engineering, Shanghai Electrochemical Energy Devices Research Center, Shanghai Jiao Tong University, Shanghai 200240, China (e-mail:

model mismatch lies in the difference between the battery model under testing operation conditions and that under unseen operation conditions, namely dynamic characteristics difference [10]. Finally, the battery aging, which continually induces the internal resistance increase and usable capacity loss along with the battery life, would lead to the model mismatch in time scale [11]. It could be seen that the model mismatch issues are unavoidable in both manufacture process and operation process, and they have been the main obstacles for the application of model-based approach in commercial BMS.

Recently, in order to improve estimation accuracy under model mismatch cases, joint and dual extended Kalman filtering (EKF) [12]–[14] as well as recursive least square (RLS) approach [15] have been widely proposed. By means of the simultaneous estimation strategy of SOC and model parameter, these approaches can provide good SOC estimates, but still have some limitations. First, most of these studies focus only on the model mismatch problem from battery aging, whereas the other two cases, i.e., battery inconsistency and battery dynamic characteristics, are rarely taken into consideration. Moreover, from an algorithmic point of view, the joint and dual EKF have the risk of failure in dealing with poor initial SOC guess [16], [17], whereas the efficiency of RLS is relatively low in combination with highly nonlinear battery models [18]. Hence, it is necessary to seek for a more robust algorithm and carry out the comprehensive investigation of model mismatch problems, especially these from battery inconsistency and battery dynamic characteristics.

Our previous work has shown that, in comparison to EKF, the moving horizon estimation (MHE) approach has faster convergence in the condition of bad initial SOC guess and can achieve more reliable estimation performance over the whole SOC range [19]. In this paper, we extend the previous works and develop the joint MHE (joint-MHE) strategy for achieving the high SOC estimation accuracy under model mismatch conditions. There are two salient contributions delivered to the literature: first, from the view of algorithm, the feasibility of joint-MHE is originally explored for accurate SOC estimation using a less accurate battery model; and second, from the view of model mismatch issues, various model mismatch cases are investigated thoroughly, i.e., the battery inconsistency, the battery dynamic characteristic difference and the combination of both. The study will provide a potential promising solution strategy for the application of model-based approach in commercial BMS. To the best of our knowledge, there are rarely related studies so far.

The structure of this paper is organized as follows. First, the state-space model is formulated based on ECM for parameter update and SOC estimation. Next, the joint-MHE strategy for SOC estimation is illustrated in detail. Then, by using the experimental datasets, the effectiveness of the proposed method is verified and the performance of joint-MHE, joint-EKF, and MHE is thoroughly compared. Finally, the main conclusions are drawn.

II. Methodology

A. Battery Model

To describe the dynamic characteristics of LIBs, various models are proposed in last decades and can be classified as electrochemical model [20], [21], equivalent circuit model (ECM) [22]–[24], and data-driven model [25]. Among them, ECM is the most widely used one in model-based approach due to its good accuracy and the low computational cost. Based on the different combination of circuit elements, such as current sources, voltage source, resistors, and resistance–capacitance (*RC*) network, the ECM can describe the battery behaviors at different model accuracy level. In general, the higher the *RC* order, the better the model accuracy and the lower the computational efficiency. Considering the balance between the model accuracy and the model complexity [19], [26], the first-order ECM is employed in this paper. The diagram of the first-order ECM is described in Fig. 1. The OCV $V_{\rm OC}$ represents the voltage source and describes the static characteristics of the battery. A resistance R_0 and an *RC* network R_1C_1 represent the ohmic effect and polarization effect during the dynamic operation respectively. *I* denotes the current source that is positive in discharging condition and negative in charging condition. All these circuit parameters are related to SOC and temperature. However, since the main aim of this paper is to verify the effectiveness of the joint-MHE-based SOC estimation method, only the SOC is considered here and all experiments are conduct at a constant temperature.

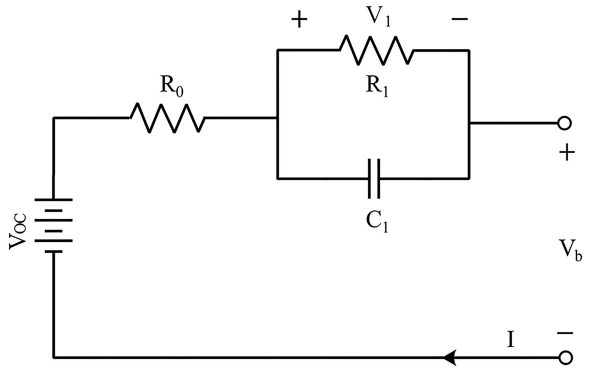

Fig. 1. Diagram of the first-order ECM.

According to the definition, the SOC at time *t* can be expressed as the ratio of remaining capacity to nominal capacity

$$\mathrm{SOC}_t = \mathrm{SOC}_0 - \frac{1}{C_n}\int_0^t I_\tau d\tau \tag{1}$$

where SOC_0 is the initial value of SOC at time t_0, and C_n is the actual capacity of a battery. Note that since the capacity loss inducing from the battery aging is out of scope of this study, all the experiments are conducted on a fresh battery and its capacity can be seen as a constant.

According to the electric circuit analysis, the battery dynamic behavior modeled by the first-order ECM can be written as follows:

$$\frac{dV_1}{dt} = \frac{I}{C_1} - \frac{V_1}{R_1C_1} \tag{2}$$

$$V_b = V_{\rm OC}(\mathrm{SOC}) - V_1 - IR_0 \tag{3}$$

where V_1 is the polarization voltage across R_1C_1 and V_b is the battery terminal voltage. $V_{\rm OC}(\mathrm{SOC})$ refers to an analytical OCV function of SOC, which is parameterized by using a monotone

polynomial OCV model as follows [27]:

$$V_{\mathrm{OC}}(\mathrm{SOC}) = \sum_{j=0}^{M} \alpha_j \mathrm{SOC}^j \tag{4}$$

where α_j is the polynomial coefficient and *M* is the polynomial order. During the battery operation, α_j can be seen as an invariant constant for a specific battery without consideration of aging effect.

Hence, the complete battery dynamic model is obtained. For the efficient integration with state estimation algorithms, (1) and (2) are transformed into their analytical forms over time interval $[t_k, t_{k+1}]$ and are expressed as (5) and (6), respectively

$$\mathrm{SOC}_{k+1} = \mathrm{SOC}_k - \frac{I_k \Delta t}{C_n} \tag{5}$$

$$V_{1,k+1} = V_{1,k} \exp\left(-\frac{\Delta t}{\tau_{1,k}}\right) + I_k R_{1,k}\left[1 - \exp\left(-\frac{\Delta t}{\tau_{1,k}}\right)\right] \tag{6}$$

where Δt presents the sampling time and $\tau_{1,k} = R_{1,k}C_{1,k}$ presents the time constant of *RC* network at time $t_{1,k}$. Correspondingly, the terminal voltage at time t_k can be represented as follows:

$$V_{b,k} = V_{\mathrm{OC}}(\mathrm{SOC}_k) - V_{1,k} - I_k R_{0,k}. \tag{7}$$

The time-varying circuit parameters $R_{0,k}$, $R_{1,k}$ and $C_{1,k}$ represented as SOC dependent polynomial functions are given, respectively, as follows:

$$R_{0,k} = R_0(\mathrm{SOC}_k) = \sum_{j=0}^{N} \beta_{1j} {\mathrm{SOC}_k}^j \tag{8}$$

$$R_{1,k} = R_1(\mathrm{SOC}_k) = \sum_{j=0}^{N} \beta_{2j} {\mathrm{SOC}_k}^j \tag{9}$$

$$C_{1,k} = C_1(\mathrm{SOC}_k) = \sum_{j=0}^{N} \beta_{3j} {\mathrm{SOC}_k}^j \tag{10}$$

where β_{1j}, β_{2j}, and β_{3j} are the polynomial coefficients and *N* is the polynomial order.

B. Augmented Nonlinear State-Space Model

To estimate the SOC using the model-based approach, the ECM described in (5)–(7) must be transformed into its discrete-time state-space form. If denote state vector $\boldsymbol{x}_k = [\mathrm{SOC}_k, V_{1,k}]'$, system input $u_k = I_k$, and system measurement $y_k = V_{b,k}$, the standard discrete state-space model can be expressed as follows:

$$\boldsymbol{x}_{k+1} = \boldsymbol{F}(\boldsymbol{x}_k, u_k) + \boldsymbol{w}_k \tag{11}$$

$$y_k = h(\boldsymbol{x}_k, u_k) + v_k \tag{12}$$

where $\boldsymbol{w}_k$ is the process white Gaussian noise with zero mean and covariance matrix $\boldsymbol{Q}_k$, and v_k is the measurement white Gaussian noise with zero mean and covariance matrix R_k. The nonlinear functions of $\boldsymbol{F}(\boldsymbol{x}_k, u_k)$ and $h(\boldsymbol{x}_k, u_k)$ are given, respectively, as follows:

$$\boldsymbol{F}(\boldsymbol{x}_k, u_k) = \begin{bmatrix} 1 & 0 \\ 0 & \exp\left(-\dfrac{\Delta t}{\tau_{1,k}}\right) \end{bmatrix} \begin{bmatrix} \mathrm{SOC}_k \\ V_{1,k} \end{bmatrix} + \begin{bmatrix} -\dfrac{\Delta t}{C_n} \\ R_{1,k}\left[1 - \exp\left(-\dfrac{\Delta t}{\tau_{1,k}}\right)\right] \end{bmatrix} I_k \tag{13}$$

$$h(\boldsymbol{x}_k, u_k) = V_{\mathrm{OC}}(\mathrm{SOC}_k) - V_{1,k} - I_k R_{0,k}. \tag{14}$$

Note that although the polynomial coefficients in (8)–(10) are offline identified by laboratory testing data, they would vary with batteries and dynamic testing protocols in practice. It means that if these parameters are uncorrected in a real-time manner, the SOC estimation performance would deteriorate. However, if all parameters are updated online, the computing cost would be extremely huge and optimization would be more difficult. To solve this problem, the sensitivity analysis of polynomial coefficients is conducted here for the update parameter selection. Based on the sensitivity analysis results, it could been found that a slight variation of relatively high-order polynomial coefficients in (8)–(10) would result in a significant variation of circuit parameters, and then might lead to an unstable terminal voltage prediction. Moreover, the constant terms and the circuit parameters are of the same order of magnitude. Hence, in this study, three constant terms, namely β_{10}, β_{20}, and β_{30}, are selected as the online updating parameters for compensating the circuit parameter mismatch issue. The state vector is then augmented as $\boldsymbol{z}_k = [\mathrm{SOC}_k, V_{1,k}, \beta_{10,k}, \beta_{20,k}, \beta_{30,k}]'$ and the nonlinear function in (13) is correspondingly formulated as follows:

$$\boldsymbol{F}(\boldsymbol{z}_k, u_k) = \begin{bmatrix} 1 & 0 & 0 & 0 & 0 \\ 0 & \exp\left(-\dfrac{\Delta t}{\tau_{1,k}}\right) & 0 & 0 & 0 \\ 0 & 0 & 1 & 0 & 0 \\ 0 & 0 & 0 & 1 & 0 \\ 0 & 0 & 0 & 0 & 1 \end{bmatrix} \begin{bmatrix} \mathrm{SOC}_k \\ V_{1,k} \\ \beta_{10,k} \\ \beta_{20,k} \\ \beta_{30,k} \end{bmatrix} + \begin{bmatrix} -\dfrac{\Delta t}{C_n} \\ R_{1,k}\left[1 - \exp\left(-\dfrac{\Delta t}{\tau_{1,k}}\right)\right] \\ 0 \\ 0 \\ 0 \end{bmatrix} I_k. \tag{15}$$

It could be seen that although the constant terms of polynomials serve as the additional states, the augmented state-space model in (14) and (15) is still nonlinear due to the polarization voltage calculation equation. By using this augmented nonlinear state-space model, the joint estimation of parameters and SOC could be obtained.

C. Moving Horizon Estimation

Based on the probability theory, the optimal estimate of the state at time k given $\{\boldsymbol{y}_k\}_{k=0}^{T}$ is a function F of the conditional probability density of the state given the system measurements, which is represented as $\{\hat{\boldsymbol{z}}_k\}_{k=0}^{T} = F(\rho(\boldsymbol{z}_0,\ldots,\boldsymbol{z}_T|\boldsymbol{y}_0,\ldots,\boldsymbol{y}_T))$. By using the Bayesian rule, this optimal state estimate can be transformed into the maximization of the conditional probability density as follows:

$$\{\hat{\boldsymbol{z}}_k\}_0^T = \arg\max \rho\left(\boldsymbol{z}_0,\ldots,\boldsymbol{z}_T\,|\boldsymbol{y}_0,\ldots,\boldsymbol{y}_T\right). \tag{16}$$

For the Gaussian–Markov process model in (14) and (15), maximizing $\rho(\boldsymbol{z}_0,\ldots,\boldsymbol{z}_T|\boldsymbol{y}_0,\ldots,\boldsymbol{y}_T)$ is equivalent to the full information optimization problem, which is shown as follows [29]:

$$\boldsymbol{J}\left(\{\hat{\boldsymbol{z}}_k\}_0^T\right) = \arg\min \|\boldsymbol{z}_0-\hat{\boldsymbol{z}}_0\|_{P_0}^2 + \sum_{k=0}^{T}\|y_k - h\left(\boldsymbol{z}_k,u_k\right)\|_R^2 + \sum_{k=0}^{T-1}\|\boldsymbol{z}_{k+1}-f\left(\boldsymbol{z}_k,u_k\right)\|_Q^2 \tag{17}$$

where P_0 is the weighting matrix to penalize the deviation of initial estimate. It could be seen that the computational complexity of this optimization problem would rapidly increase with the sampling time. To solve this problem, the MHE strategy is proposed [28]–[30]. By introducing a horizon length L, the entire time interval at sampling time t_T can be separated into two parts $[0,\ldots,t_{T-L}]$ and $[t_{T-L+1},\ldots,t_T]$. The full information optimization problem can be reformulated as follows:

$$\begin{aligned}\boldsymbol{J}\left(\{\hat{\boldsymbol{z}}_k\}_0^T\right) = &\arg\min \|\boldsymbol{z}_0-\hat{\boldsymbol{z}}_0\|_{P_0}^2 + \sum_{k=0}^{T-L}\|y_k - h\left(\boldsymbol{z}_k,u_k\right)\|_R^2 \\ &+ \sum_{k=0}^{T-L}\|\boldsymbol{z}_{k+1}-f\left(\boldsymbol{z}_k,u_k\right)\|_Q^2 + \sum_{k=T-L+1}^{T}\|y_k - h\left(\boldsymbol{z}_k,u_k\right)\|_R^2 \\ &+ \sum_{k=T-L+1}^{T-1}\|\boldsymbol{z}_{k+1}-f\left(\boldsymbol{z}_k,u_k\right)\|_Q^2.\end{aligned} \tag{18}$$

If we combine the former three terms into one and define it as arrival cost $\varphi_{T-L+1}(\boldsymbol{z}_{T-L+1})$ [28], [31], the joint estimation problem of parameters and SOC at time t_T can be expressed as a nonlinear constrained optimization problem in the following equations:

$$\begin{aligned}&\underset{\boldsymbol{z}_{T-L+1},\{\boldsymbol{w}_k\}_{T-L+1}^{T-1}}{\arg\min}\ \varphi_{T-L+1}\left(\boldsymbol{z}_{T-L+1}\right) \\ &\quad+\sum_{k=T-L+1}^{T}\|y_k - h\left(\boldsymbol{z}_k,u_k\right)\|_R^2 \\ &\quad+\sum_{k=T-L+1}^{T-1}\|\boldsymbol{z}_{k+1}-f\left(\boldsymbol{z}_k,u_k\right)\|_Q^2\end{aligned} \tag{19}$$

$$\text{s.t. } \varphi_{T-L+1}\left(\boldsymbol{z}_{T-L+1}\right) = \|\boldsymbol{z}_{T-L+1}-\bar{\boldsymbol{z}}_{T-L+1}\|_{P_{T-L+1}}^2 \tag{20}$$

$$\begin{aligned}\begin{bmatrix}\mathrm{SOC}_{k+1}\\ V_{1,k+1}\\ \beta_{10,k+1}\\ \beta_{20,k+1}\\ \beta_{30,k+1}\end{bmatrix} &= \begin{bmatrix}1 & 0 & 0 & 0 & 0\\ 0 & \exp\left(-\dfrac{\Delta t}{\tau_{1,k}}\right) & 0 & 0 & 0\\ 0 & 0 & 1 & 0 & 0\\ 0 & 0 & 0 & 0 & 1\\ 0 & 0 & 0 & 0 & 1\end{bmatrix}\begin{bmatrix}\mathrm{SOC}_k\\ V_{1,k}\\ \beta_{10,k}\\ \beta_{20,k}\\ \beta_{30,k}\end{bmatrix} \\ &+\begin{bmatrix}-\dfrac{\Delta t}{C_n}\\ R_{1,k}\left[1-\exp\left(-\dfrac{\Delta t}{\tau_{1,k}}\right)\right]\\ 0\\ 0\\ 0\end{bmatrix} I_k + \begin{bmatrix}w_{1,k}\\ w_{2,k}\\ w_{3,k}\\ w_{4,k}\\ w_{5,k}\end{bmatrix}\end{aligned}$$

$$k = T-L+1,\ldots,T \tag{21}$$

$$\begin{aligned}V_{b,k} &= V_{\mathrm{OC}}(\mathrm{SOC}_k) - V_{1,k} - I_k R_{0,k} + v_{1,k},\\ &\quad\times k = T-L+1,...,T\end{aligned} \tag{22}$$

$$R_{0,k} = \beta_{10,k} + \sum_{j=1}^{N}\beta_{1j}{\mathrm{SOC}_k}^j, k = T-L+1,...,T \tag{23}$$

$$R_{1,k} = \beta_{20,k} + \sum_{j=1}^{N}\beta_{2j}{\mathrm{SOC}_k}^j, k = T-L+1,...,T \tag{24}$$

$$C_{1,k} = \beta_{30,k} + \sum_{j=1}^{N}\beta_{3j}{\mathrm{SOC}_k}^j, k = T-L+1,...,T \tag{25}$$

$$\tau_{1,k} = R_{1,k}C_{1,k}, k = T-L+1,...,T \tag{26}$$

$$0 \le \mathrm{SOC}_k \le 1, k = T-L+1,...,T \tag{27}$$

where $\bar{\boldsymbol{z}}_{T-L+1}$ presents the prior estimate of states at time t_{T-L+1}. The constraints in (27) are used to ensure the reasonable estimated values of SOC. Generally, the covariance matrices Q and R are considered as constants in the estimation process, covariance matrix P is iteratively updated using the EKF method shown in as follows [32]:

$$\begin{aligned}P_{k+1} = B_kQ_kB_k' + A_k(P_k - P_kC_k'\\ \times(R_k + C_kP_kC_k')^{-1}C_kP_k)A_k'\end{aligned} \tag{28}$$

where A_k is the Jacobian matrices of $f(\boldsymbol{z}_k,u_k)$ with respect to states. B_k is the Jacobian matrices of $f(\boldsymbol{z}_k,u_k)$ with respect to noises. C_k is the Jacobian matrix of $h(\boldsymbol{z}_k,u_k)$ with respect to states.

According to the above descriptions, it could be seen that every estimation in the MHE strategy only relies on the latest L measurements, whereas the past measurement information is summarized in the arrival cost. By repeatedly solving the finite horizon optimization problem defined in (19)–(27), the joint-MHE can realize the simultaneous parameter and state estimation in a real-time manner.

Fig. 2 depicts the flowchart of the proposed strategy. The offline battery model is first built by identifying the polynomial functions of circuit parameters in ECM. Then, by the sensitivity analysis, the update parameters are selected and added to the

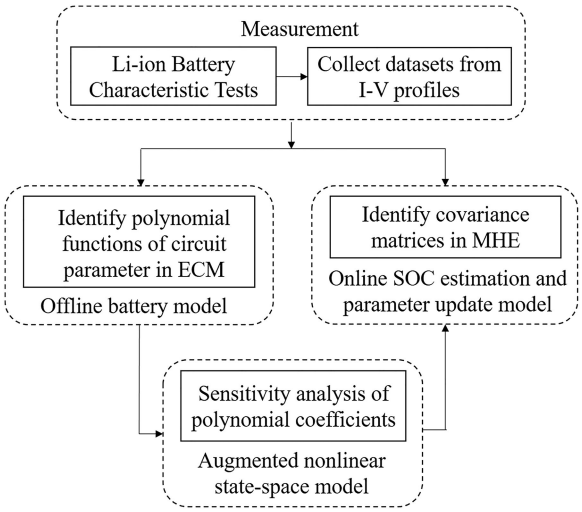

Fig. 2. Flowchart of the joint-MHE model construction for online SOC estimation and parameter update.

state-space model as additional states. Finally, after optimizing the covariance matrices of process and measurement noises, the joint-MHE model is established and then conducted for the online SOC estimation and parameter update. Both offline battery model and online estimation model are constructed based on the collected datasets from I–V profiles of LIBs.

Here, two criteria including the root-mean-square error (RMSE) and absolute error (AE) are used to evaluate the SOC estimation performance of the proposed method

$$RMSE = \sqrt{\frac{\sum_{k=1}^{T} \left| \hat{\mathrm{SOC}}_k - \mathrm{SOC}_k \right|^2}{T}} \tag{29}$$

$$AE_k = \left| \hat{\mathrm{SOC}}_k - \mathrm{SOC}_k \right| \tag{30}$$

where $\hat{\mathrm{SOC}}_k$ is the estimated value of SOC_k.

III. Experimental

The testing datasets are acquired through the battery test bench, which comprises a battery test system, a programmable temperature test chamber, and a host computer for programming test profile and storing experimental data. The measurement accuracy of current and voltage is 0.05% and logged at frequency of 1 Hz. The tested battery is an NMC LIB with 20-Ah nominal capacity, 3.6 V nominal voltage. The battery test bench conducts four typical characteristic tests at 298 K, including the discharge capacity test, the constant current discharge test (CCDT), a hybrid pulse power characterization (HPPC) test, and a dynamic stress test (DST). Before every test, the battery is rested for 2 h after charged to its full capacity.

The HPPC test is used to establish the offline model, identify the tuning parameters, and investigate the performance of the joint-MHE approach in condition of battery inconsistency. Fig. 3(a) shows the voltage response profile composed of one HPPC cycle and one 1.0C-rate discharge period. In each HPPC cycle, the battery is first discharged by 2.5C-rate current for 10 s and then charged by 2.0C-rate current for 10 s after a 40-s rest. In each 1.0C-rate discharge period, the battery is discharged to the preset SOC. The complete HPPC test from 100% to 0% SOC is shown in Fig. 3(b), which is composed of the repetition of HPPC cycle, 1.0C-rate discharge period, and rest periods. The DST and CCDT are performed to further validate the SOC estimation performance. Fig. 4(a) shows the voltage response profile of one DST cycle with seven discrete power levels. The entire DST composed of repeated DST cycle from 100% to 10% SOC is shown in Fig. 4(b). The CCDTs are conducted at three discharge rates over the whole SOC range, including 0.5C-rate, 1.0C-rate, and 1.2C-rate.

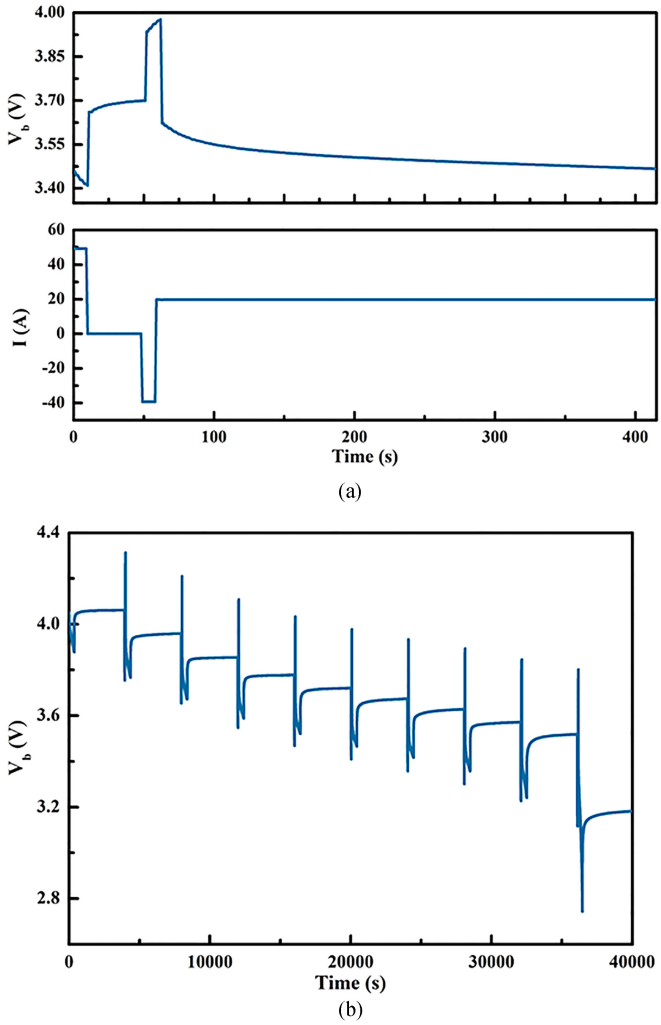

Fig. 3. HPPC test. (a) One HPPC cycle followed 1C-rate discharge period. (b) Voltage response of complete HPPC test.

IV. Results and Discussion

The offline battery model construction and tuning parameter identification in joint-MHE are first performed on the HPPC test datasets. Then, the SOC estimation performance of joint-MHE in model mismatch cases is thoroughly evaluated based on the datasets from CCTDs, HPPC, and DST, and compared to that

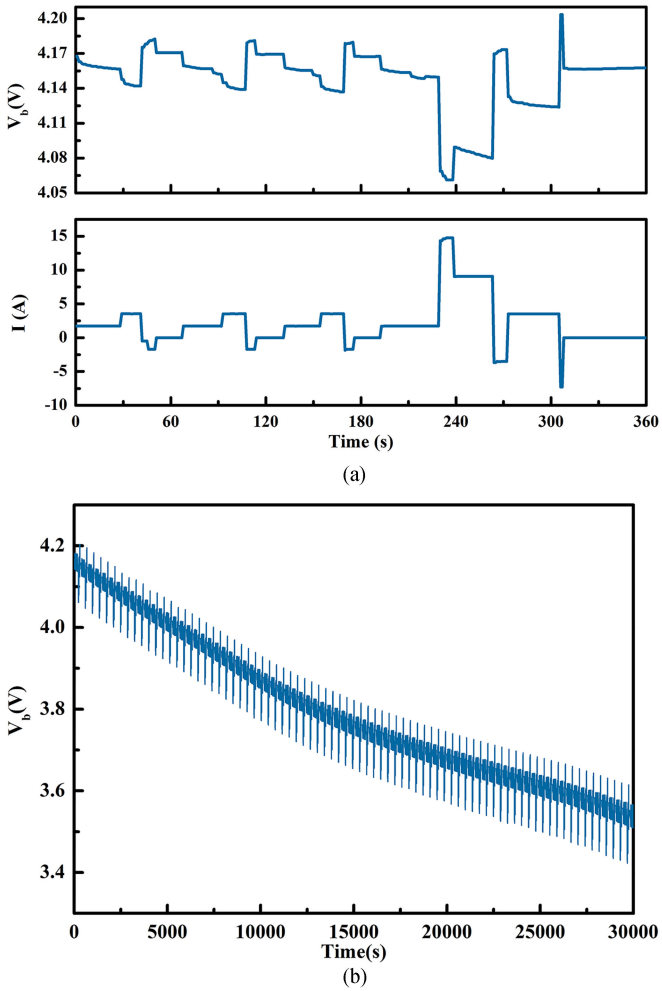

Fig. 4. DST test. (a) One DST cycle. (b) Voltage response of complete DST test.

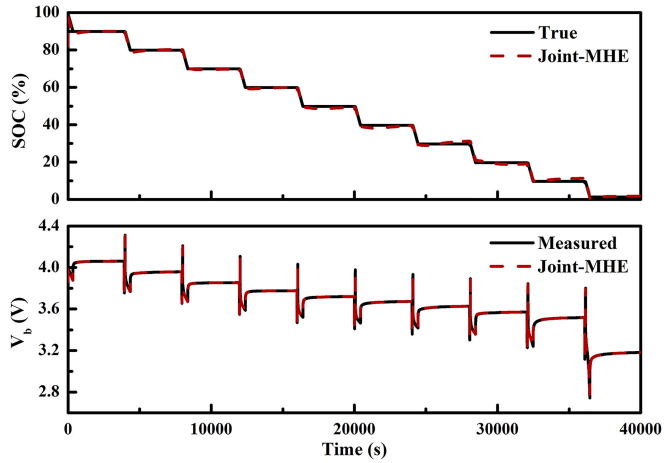

Fig. 5. Results of SOC estimation and battery voltage estimation using joint-MHE for the HPPC test.

of joint-EKF and MHE. All the three algorithms are coded and implemented in MATLAB.

The detailed procedure of offline model construction and tuning parameter determination is available in the previous work [19]. The covariance matrices in joint-MHE are optimized as: $P = \text{diag}(100\ 0.1\ 0.01\ 0.1\ 100000)$, $Q = \text{diag}(0.01\ 0.001\ 0.001\ 0.01\ 1000)$, and $R = 1000$. The horizon length L is set as 20. Fig. 5 shows the joint-MHE estimation results during the complete HPPC profile. It could be seen that the estimated SOC is almost the same as the true SOC and the corresponding RMSE value of SOC is 0.77%, and the estimated battery voltage could well match the measured voltage and the corresponding RMSE value of battery voltage is 2.8 mV.

The following section will thoroughly investigate the effectiveness of the joint-MHE approach in three model mismatch conditions, i.e., battery inconsistency, battery dynamic characteristics difference, and the combination of both. Moreover, two methods, i.e., joint-EKF and MHE, are utilized here for the performance comparisons. To make it fair, the covariance matrices in joint-EKF and MHE are also optimized based on HPPC test datasets. The covariance matrices in MHE are set as: $P = \text{diag}(100\ 1)$, $Q = \text{diag}(0.1\ 0.01)$, and $R = 10$, and those in joint-EKF are set as: $P = \text{diag}(1000\ 1\ 0.01\ 1\ 100000)$, $Q = \text{diag}(1000\ 1\ 0.01\ 1\ 100000)$, and $R = 1000$. Considering that the true initial SOC value is hard to obtain in practical, the initial SOC guess is fixed to 50%, no matter what the true SOC value is.

A. *Battery Dynamic Characteristics Difference*

The CCDT and HPPC tests have great dynamic characteristics difference. Therefore, when we use the offline ECM model based on HPPC test dataset to predict the terminal voltage responses of CCDT test, the RMSE values of voltage would reach up to 73.3, 29.2, and 38.0 mV for 0.5C-rate, 1.0C-rate, and 1.2C-rate, respectively. It illustrates that without properly tuning the parameters, the offline constructed model might produce large model prediction error in other operation protocols. To validate the effectiveness of the proposed method in model mismatch condition, the joint-MHE is conducted in three CCDT cases and compared to the joint-EKF and the MHE. The SOC estimation comparisons are, respectively, shown in Fig. 6(a), (c), and (e), the corresponding AE comparisons are, respectively, shown in Fig. 6(b), (d), and (f), and the RMSE results are summarized in Table I.

From Fig. 6(a), (c), and (e), it is observed that the estimated SOC profiles of MHE deviate from the true SOC in 1.0C-rate and 1.2C-rate CCDT cases, whereas the estimated SOC profiles of joint-MHE and joint-EKF can well match with the true SOC in all three cases. Particularly in 1.2C-rate CCDT case, it could be found that MHE still produces the obvious deviation after tracking the first several SOC values. The main reason is the dynamic characteristics difference during the operation range. At first seconds, the model mismatch level might be relatively low and within the robustness ability of MHE. However, along with the battery operation, the parameter mismatch problem becomes more and more serious until beyond the MHE ability. It illustrates that without online parameter correction, the MHE has a risk of failure to accurately estimate SOC in the unseen operational conditions. In contrast, joint-MHE and joint-EKF can provide the high SOC estimation accuracy due to the

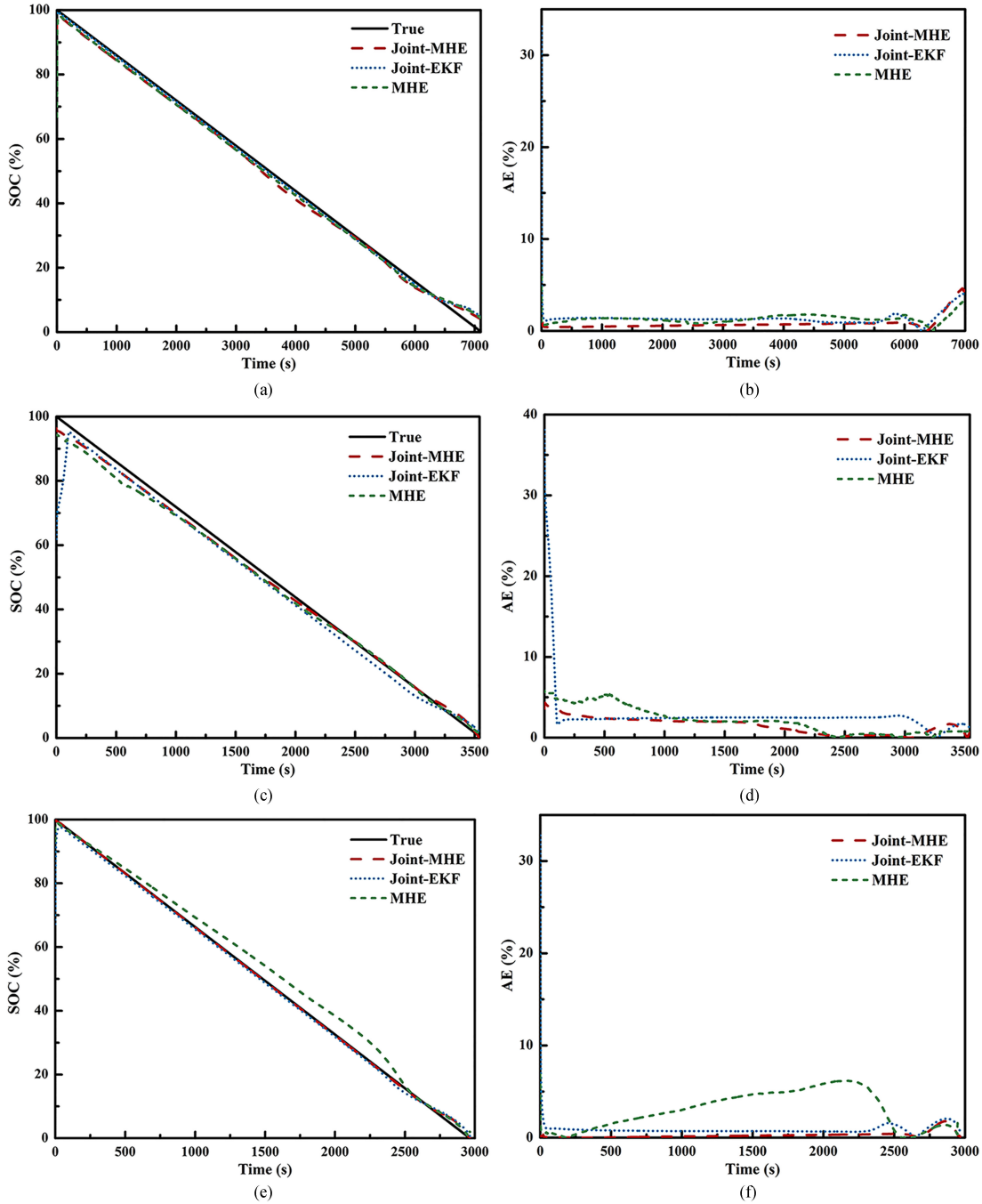

Fig. 6. Comparison of SOC estimation results and AE in three CCDT cases with SOC_0 guess of 50%. (a) and (b) 0.5C-rate. (c) and (d) 1.0C-rate. (e) and (f) 1.2C-rate.

TABLE I
RMSE COMPARISON OF JOINT-MHE, JOINT-EKF, AND MHE IN THREE CCDT CASES WITH SOC_0 GUESS OF 50%

	0.5C-rate	1.0C-rate	1.2C-rate
joint-MHE	1.19%	1.46%	0.42%
joint-EKF	1.60%	4.17%	1.21%
MHE	1.32%	2.64%	3.41%

effectiveness of simultaneous parameter and state estimation strategy in reducing the adverse effect of model mismatch issue on estimation. Furthermore, Fig. 6(b), (d), and (f) show that in all three CCDT cases, joint-MHE generally produces smaller errors than joint-EKF over the whole range. The same results also can be drawn in Table I. Take 1.0C-rate CCDT case as an example, the RMSE value of joint-EKF is 4.17%, whereas that of joint-MHE is only 1.46%. This implies that the optimization estimation strategy allows joint-MHE to achieve the higher accuracy than joint-EKF.

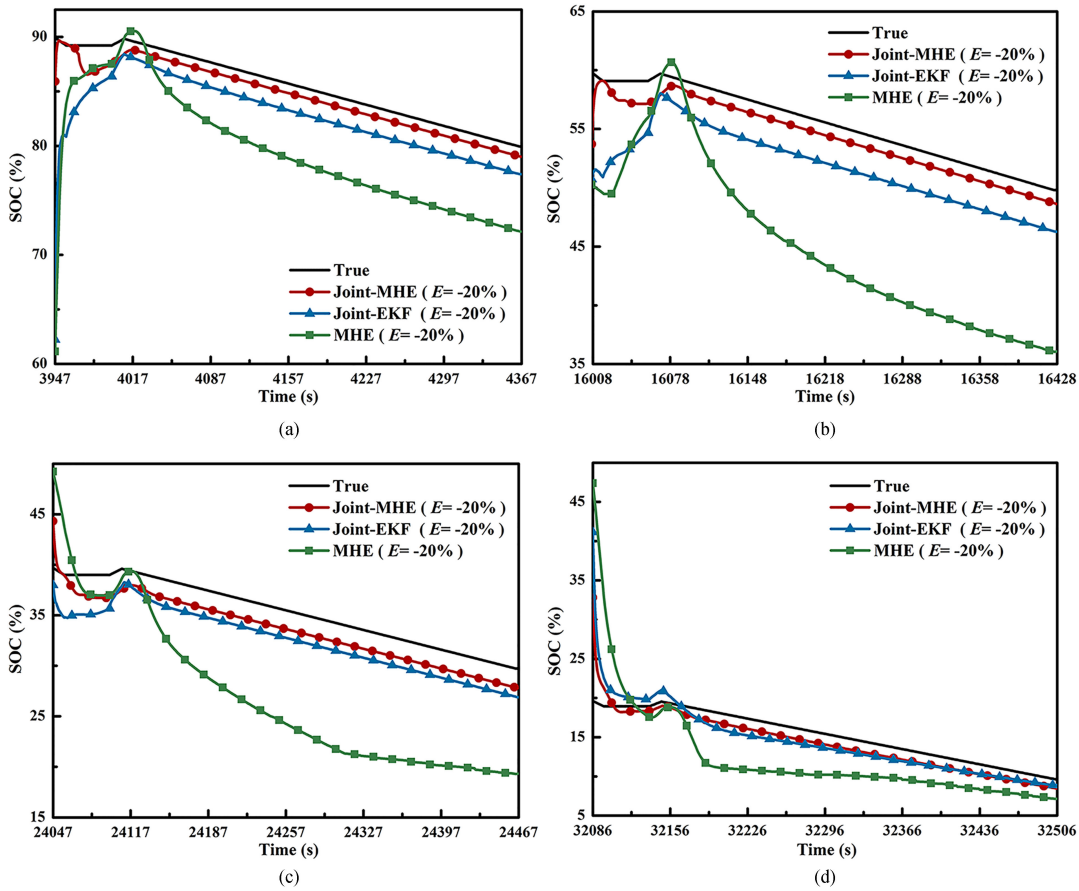

Fig. 7. Comparison of SOC estimation results in four HPPC cases with parameter bias of -20% and SOC_0 guess of 50%. (a) $\mathrm{SOC}_0 = 90\%$. (b) $\mathrm{SOC}_0 = 60\%$. (c) $\mathrm{SOC}_0 = 40\%$. (d) $\mathrm{SOC}_0 = 20\%$.

In addition, Fig. 6(a), (c), and (e) illustrate that joint-MHE and MHE are able to recover from the bad initial SOC guess within several seconds in CCDT cases, which is much faster than joint-EKF. This observation is also confirmed by the AE profiles in Fig. 6(b), (d), and (f). Take 1.0C-rate CCDT case as an example, the SOC estimation errors of MHE and joint-MHE could drop to 5% after the few first seconds, whereas joint-EKF takes about 100 s to achieve such a low estimation error level. The faster convergence speed of MHE and joint-MHE approaches illustrates that the optimization-based estimation approach is more effective than the iterative update based approach. Moreover, compared to EKF, which has only current observation for updating, the utilization of more measurements in one estimation makes MHE provide better estimation accuracy and faster convergence speed.

All the CCDT comparison results demonstrate that, profiting from the strategy of simultaneous parameter and state estimation, joint-MHE could effectively tackle the model mismatch problem originating from the battery dynamic characteristics difference, and achieve much faster and more accurate SOC estimation in the poor initial guess condition.

B. Battery Inconsistency

The battery inconsistency is another important origin of model mismatch. In an ECM, circuit parameters, i.e., the ohmic resistance R_0, polarization resistance R_1, and capacitance C_1, always vary with batteries, yielding the model parameter variation in battery-to-battery. Considering that the circuit parameters and their corresponding polynomial constant terms are of the same order of magnitude, the polynomial constant terms are used as the variation parameters here. Furthermore, to characterize the different model mismatch degrees, 4% biases, i.e., $\pm 10\%$, $\pm 20\%$, $\pm 30\%$, and $\pm 40\%$ are added to the nominal values of polynomial constant terms. E is used to denote the percentage bias for simplicity.

The comparisons of SOC estimation results in four HPPC cases with parameter biases of -20% and $+20\%$ are shown in Figs. 7 and 8, respectively. It is observed that MHE almost fails to converge to the true SOC in all cases, whereas joint-MHE and joint-EKF are able to provide stable and satisfactory estimates. These results indicate that both underestimation and overestimation of model parameters could significantly deteriorate the SOC estimation performance, and the strategy of simultaneous parameter and state estimation is an effective way to handle this problem. Furthermore, compared to joint-EKF, joint-MHE could provide more accurate SOC estimation and recover from the incorrect initial SOC guess within less time, which benefits from both the utilization of sufficient enough information and the adoption of optimization strategy. Moreover, for the negative parameter bias of -20%, joint-MHE and joint-EKF show the slight underestimates in all cases, whereas for the positive

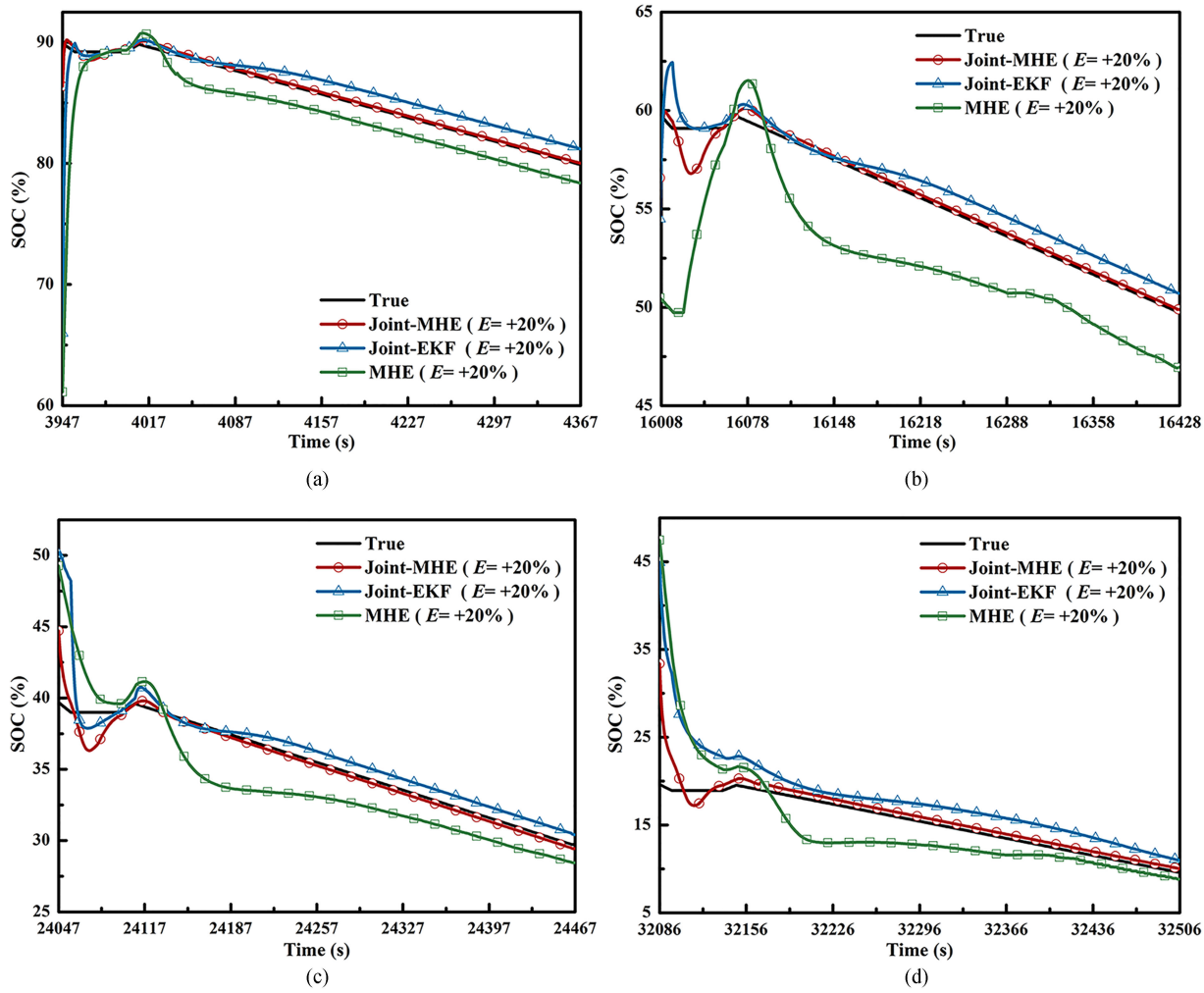

Fig. 8. Comparison of SOC estimation results in four HPPC cases with parameter bias of +20% and SOC_0 guess of 50%. (a) $SOC_0 = 90\%$. (b) $SOC_0 = 60\%$. (c) $SOC_0 = 40\%$. (d) $SOC_0 = 20\%$.

TABLE II
RMSE COMPARISON OF JOINT-MHE, JOINT-EKF, AND MHE IN FOUR HPPC CASES WITH PARAMETER BIASES OF ±20% AND SOC_0 GUESS OF 50%

SOC_0	90%		60%		40%		20%	
E	-20%	+20%	-20%	+20%	-20%	+20%	-20%	+20%
Joint-MHE	1.06%	0.48%	1.22%	0.71%	1.86%	0.88%	1.54%	1.32%
Joint-EKF	3.44%	1.68%	3.89%	0.90%	2.83%	1.77%	2.26%	3.96%
MHE	6.68%	2.92%	11.13%	3.75%	9.64%	2.60%	5.66%	4.72%

parameter bias of +20%, joint-MHE could almost perfectly match the true SOC after the convergence.

Table II shows the RMSE comparison among joint-MHE, joint-EKF, and MHE in four HPPC cases with parameter bias of ±20%. From Table II, it is found that the RMSE values of joint-MHE are obviously smaller than that of joint-EKF and MHE in all cases. The maximum RMSE of joint-EKF and MHE are 3.96% and 11.13%, respectively, whereas that of joint-MHE is only 1.86%. All the results show that the joint estimation algorithms are much less sensitive to the model mismatch problem originating from battery inconsistency and can provide more accurate SOC estimates. Moreover, although both joint-MHE and joint-EKF show the satisfactory accuracy, joint-MHE seem to be favored due to its better stability and faster convergence. The higher accuracy of joint methods results from the parameter update strategy, whereas the lowest error of joint-MHE is due to the way of using sufficient measurements in one estimation.

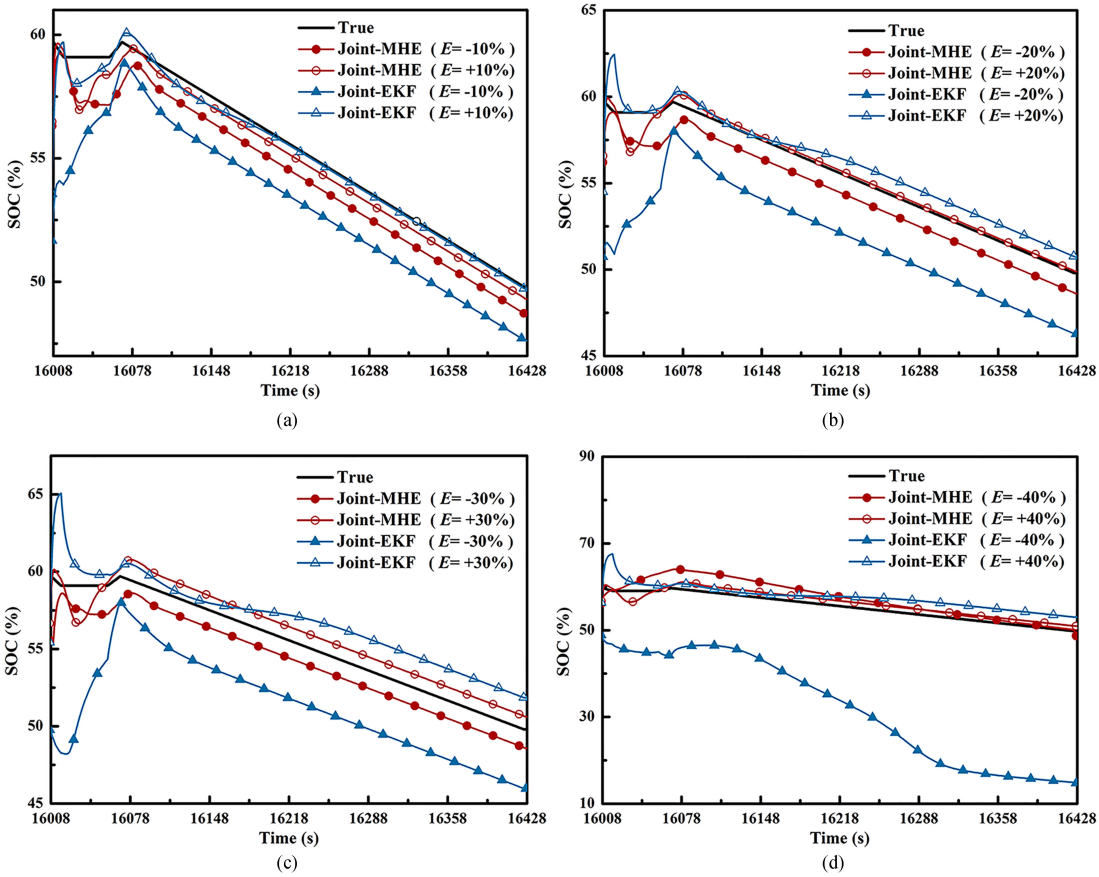

Fig. 9. Comparison of SOC estimation results in HPPC cycle with SOC_0 of 60% and SOC_0 guess of 50% in different parameter bias cases. (a) $E = \pm 10\%$. (b) $E = \pm 20\%$. (c) $E = \pm 30\%$. (d) $E = \pm 40\%$.

TABLE III
RMSE COMPARISON OF JOINT-MHE AND JOINT-EKF IN HPPC CYCLE WITH SOC_0 OF 60% AND SOC_0 GUESS OF 50% IN DIFFERENT PARAMETER BIAS CASES

E	-10%	+10%	-20%	+20%	-30%	+30%	-40%	+40%
Joint-MHE	1.15%	0.61%	1.22%	0.51%	1.28%	0.99%	2.52%	1.27%
Joint-EKF	2.39%	0.50%	3.89%	0.90%	4.57%	1.77%	25.02%	2.67%

To further investigate the model correction ability of joint-MHE and joint-EKF, two joint estimation methods are then applied to the HPPC cycle with SOC_0 of 60% in different parameter bias cases, i.e., $\pm 10\%$, $\pm 20\%$, $\pm 30\%$, and $\pm 40\%$. The SOC estimation comparisons are shown in Fig. 9, and the corresponding RMSEs are summarized in Table III. From Fig. 9, it is observed that although the estimation accuracy of both methods generally decreases with the increasing of parameter bias degree, joint-MHE can accurately track the true SOC profile in all cases, whereas joint-EKF fails to converge when parameter bias reaches -40%. Moreover, joint-MHE shows the better convergence performance. From Table III, it is found that two joint estimation methods have the comparable estimation accuracy in the positive biases cases, whereas joint-MHE has higher accuracy in the negative biases cases, especially the large negative bias case. Take parameter biases

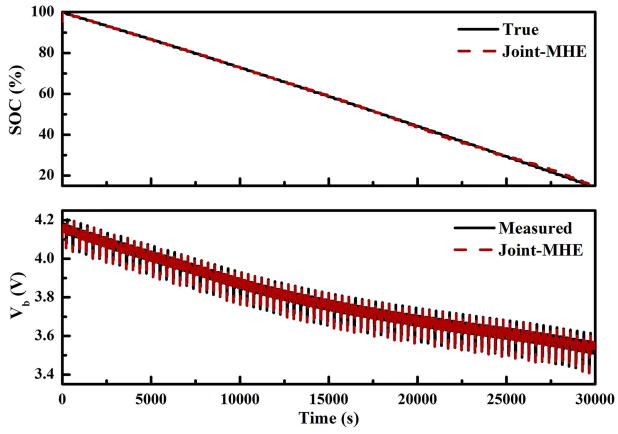

Fig.10. Results of SOC estimation and battery voltage estimation using joint-MHE for the DST test with SOC_0 guess of 50%.

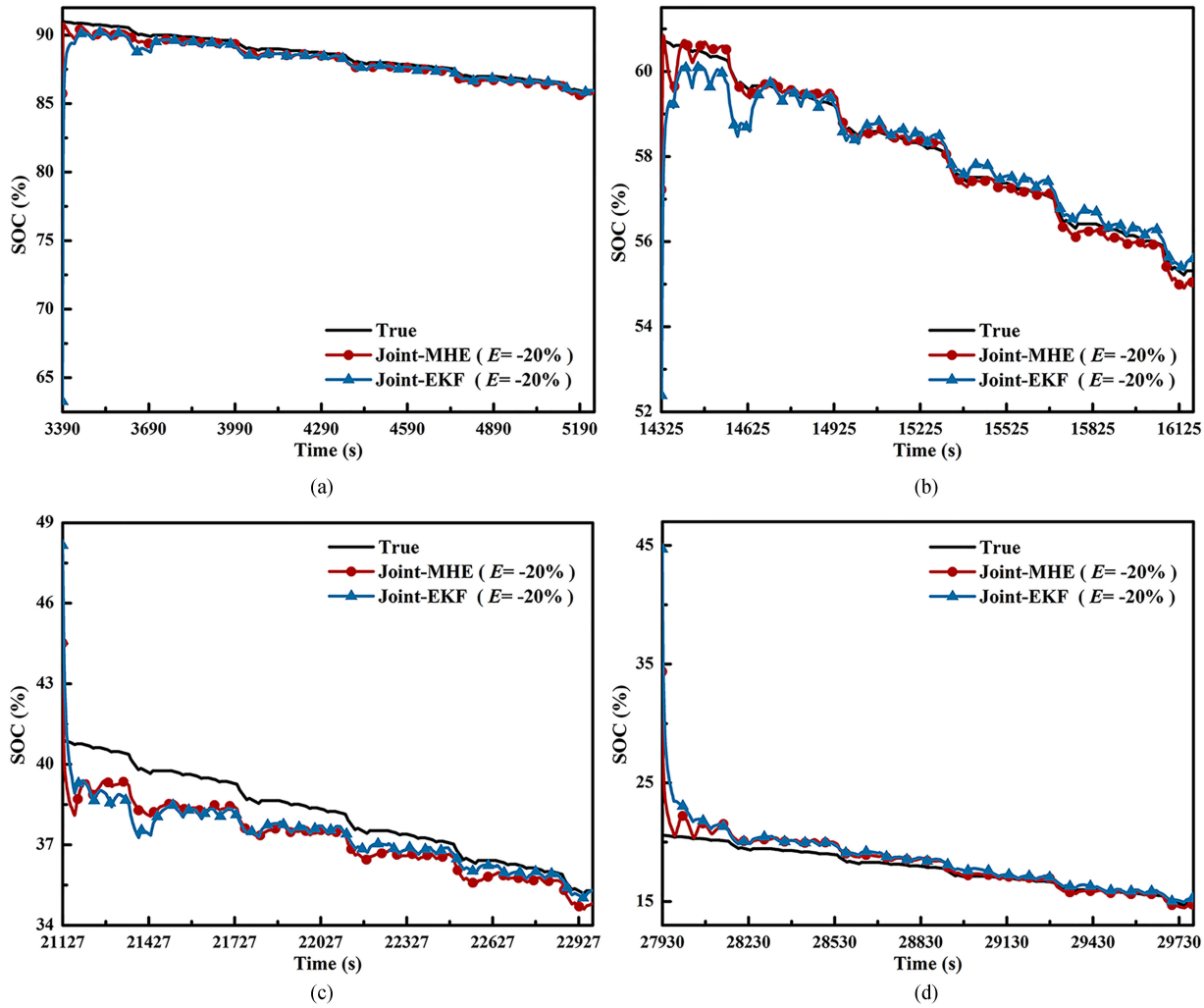

Fig. 11. Comparison of SOC estimation results in four DST cases with parameter bias of −20% and SOC_0 guess of 50%. (a) $SOC_0 = 90\%$. (b) $SOC_0 = 60\%$. (c) $SOC_0 = 40\%$. (d) $SOC_0 = 20\%$.

of −30% and −40% as examples, the RMSEs of joint-EKF are 4.57% and 25.02%, respectively, whereas those of joint-MHE are only 1.28% and 2.52%, respectively. These comparison results imply that joint-MHE possesses a stronger ability of model parameter correction in the case of higher degree of model mismatch. It could be reasonable to say that compared to joint-EKF, joint-MHE has a stronger robustness and can provide a more reliable and accurate SOC estimation when there exist model parameter biases originating from battery inconsistency.

C. Combination of Battery Inconsistency and Battery Dynamic Characteristics Difference

Compared to the HPPC profile in Fig. 3, the DST profile in Fig. 4 shows more complex dynamic characteristics and consequently used to validate the effectiveness of joint-MHE under the variable power discharge regimes.

The estimation results in Fig. 10 show that the estimated SOC is almost the same as the true SOC and the corresponding RMSE value of SOC is 0.78%, and the estimated battery voltage could well match the measured voltage and the corresponding RMSE value of battery voltage is 3.2 mV. It again demonstrates that joint-MHE could effectively perform accurate SOC estimation with complex fast dynamic operation regimes.

Then, to further explore the performance of joint-MHE in the presence of model mismatch mainly from battery inconsistency, four DST cycles with SOC_0 of 90%, 60%, 40%, and 20% and two parameter biases of −20% and +20% are studied. Figs. 11 and 12 show the SOC estimation comparison of joint-MHE and joint-EKF in four DST cases with parameter biases of −20% and +20%, respectively. Table IV summarizes the corresponding RMSEs. It is observed that although both algorithms can provide the satisfactory SOC estimates in all cases, joint-MHE performs better in terms of estimation accuracy and convergence speed. Moreover, for the case in which both algorithms have the comparable SOC estimation accuracy, joint-MHE can estimate the battery voltage more accurately, especially in the presence of abrupt changes in voltage responses. This observation is shown in Fig. 13(a) and (b). Again, stronger robustness of joint-MHE is demonstrated.

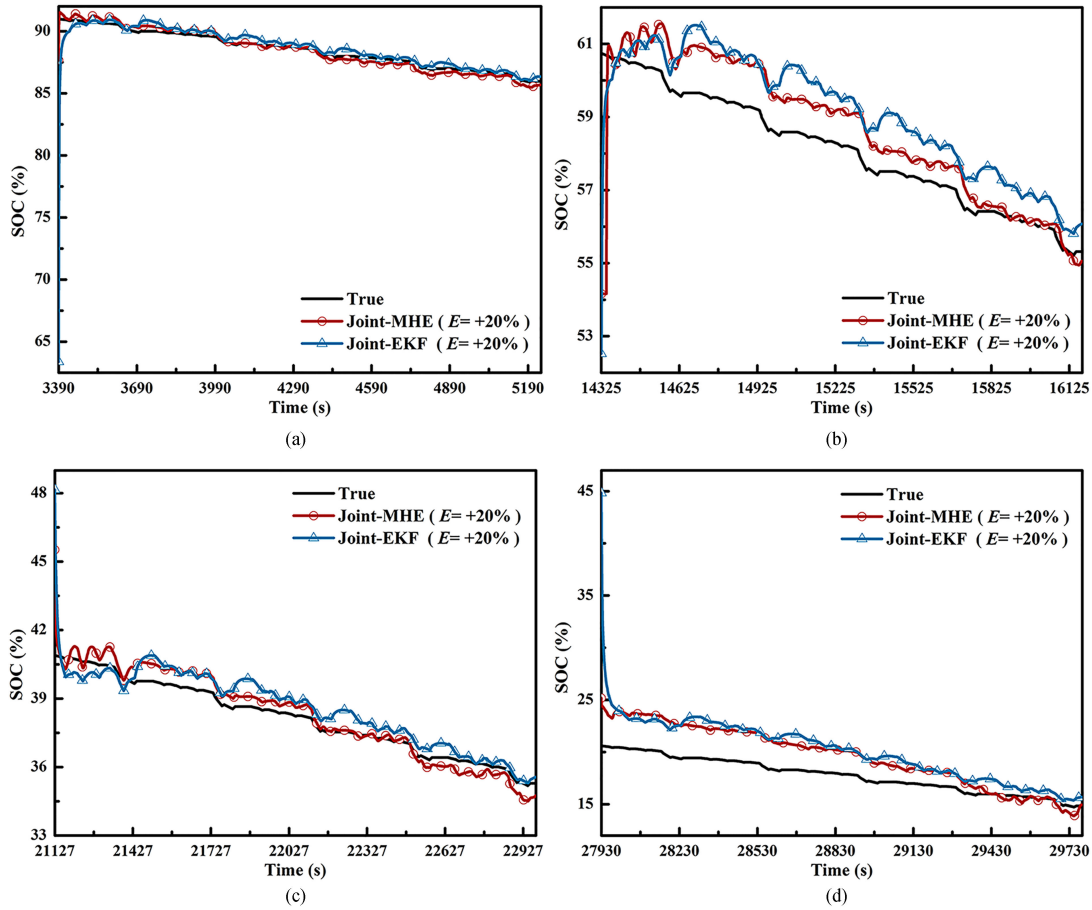

Fig. 12. Comparison of SOC estimation results in four DST cases with parameter bias of +20% and SOC_0 guess of 50%. (a) $SOC_0 = 90\%$. (b) $SOC_0 = 60\%$. (c) $SOC_0 = 40\%$. (d) $SOC_0 = 20\%$.

TABLE IV
RMSE COMPARISON OF JOINT-MHE, JOINT-EKF, AND MHE IN FOUR DST TESTS WITH PARAMETER BIAS OF ±20% AND SOC_0 GUESS OF 50%

SOC_0	90%		60%		40%		20%	
E	-20%	+20%	-20%	+20%	-20%	+20%	-20%	+20%
Joint-MHE	0.79%	0.70%	0.61%	1.35%	1.22%	0.79%	0.90%	2.25%
Joint-EKF	1.28%	1.22%	0.92%	1.52%	1.28%	0.91%	1.50%	2.81%

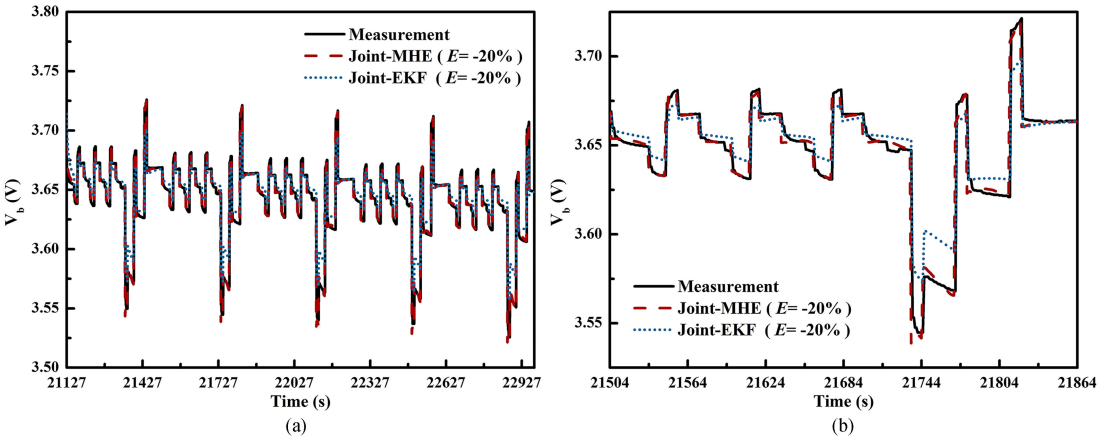

Fig. 13. Results of battery voltage estimation. (a) For 40% DST test with parameter bias of −20%. (b) For one enlarged DST cycle during the 40% DST test.

V. Conclusion

To effectively tackle model mismatch issues, the joint-MHE approach that can simultaneously estimate the model parameter and state is proposed here. In this paper, the circuit-equivalent battery model is first constructed by parameterizing the circuit parameters as polynomial function of SOC. Then, by the sensitivity analysis, the update parameters are selected and added to the state-space model as additional states. Finally, the joint-MHE strategy is conducted for the simultaneous parameter and SOC estimation. To investigate the performance of the proposed method thoroughly, three model mismatch conditions are considered, including battery inconsistency, battery dynamic characteristics difference, and the combination of both. Moreover, two methods, i.e., joint-EKF and MHE, are utilized for the performance comparisons. It is observed that MHE cannot converge in most cases due to the lack of online parameter correction, whereas both joint strategies can provide relatively accurate and reliable SOC estimation. Furthermore, in the comprehensive comparison of two joint methods, joint-MHE shows the better estimation performance. First, the joint-MHE has stronger model correction ability. In relatively extreme battery inconsistency case, such as the parameter bias of -40% in HPPC, the joint-EKF fails, whereas the joint-MHE can still conduct the accurate and reliable estimation. Second, joint-MHE can generally provide more accurate and stable SOC estimation. Even in some cases where the SOC estimation performance of both are comparable, joint-MHE can track the battery voltage much better. Finally, in face of bad initial SOC guess, joint-MHE shows faster convergence speed and stronger robustness. The SOC estimation RMSE of joint-MHE is smaller than 2% in most cases. To conclude, the proposed joint-MHE can be seen as an effective method for the accurate and reliable SOC estimation in the presence of model mismatch, and consequently would be a potential promising solution for real application of model-based SOC estimation approach in commercial BMS.

References

[1] P. Jochem, C. Doll, and W. Fichtner, "External costs of electric vehicles," *Transp. Res. Part D, Transp. Environ.*, vol. 42, pp. 60–76, Jan. 2016.

[2] C. M. Martinez, X. Hu, D. Cao, E. Velenis, B. Gao, and M. Wellers, "Energy management in plug-in hybrid electric vehicles: Recent progress and a connected vehicles perspective," *IEEE Trans. Veh. Technol.*, vol. 66, no. 6, pp. 4534–4549, Jun. 2017.

[3] M. A. Hannan, M. S. H. Lipu, A. Hussain, and A. Mohamed, "A review of lithium-ion battery state of charge estimation and management system in electric vehicle applications: Challenges and recommendations," *Renewable Sustain. Energy Rev.*, vol. 78, pp. 834–854, Oct. 2017.

[4] K. S. Ng, C.-S. Moo, Y.-P. Chen, and Y.-C. Hsieh, "Enhanced coulomb counting method for estimating state-of-charge and state-of-health of lithium-ion batteries," *Appl. Energy*, vol. 86, pp. 1506–1511, Sep. 2009.

[5] Y. Xing, W. He, M. Pecht, and K. L. Tsui, "State of charge estimation of lithium-ion batteries using the open-circuit voltage at various ambient temperatures," *Appl. Energy*, vol. 113, pp. 106–115, Jan. 2014.

[6] A. Farmann, W. Waag, A. Marongiu, and D. U. Sauer, "Critical review of on-board capacity estimation techniques for lithium-ion batteries in electric and hybrid electric vehicles," *J. Power Sources*, vol. 281, pp. 114–130, Jun. 2016.

[7] G. Fathoni, S. A. Widayat, P. A. Topan, A. Jalil, A. I. Cahyadi, and O. Wahyunggoro, "Comparison of State-of-Charge (SOC) estimation performance based on three popular methods: Coulomb counting, open circuit voltage, and Kalman filter," in *Proc. 2nd Int. Conf. IEEE Automat., Cogn. Sci. Opt. Micro Elect.-Mech. Syst. Inf. Technol.*, 2017, pp. 70–74.

[8] M. A. Roscher, O. S. Bohlen, and D. U. Sauer, "Reliable state estimation of multicell lithium-ion battery systems," *IEEE Trans. Energy Convers.*, vol. 26, no. 3, pp. 737–743, Sep. 2011.

[9] Y. Zheng *et al.*, "Cell state-of-charge inconsistency estimation for $LiFePO_4$ battery pack in hybrid electric vehicles using mean-difference model," *Appl. Energy*, vol. 111, pp. 571–580, Nov. 2013.

[10] R. Xiong, F. Sun, Z. Chen, and H. He, "A data-driven multi-scale extended Kalman filtering based parameter and state estimation approach of lithium-ion olymer battery in electric vehicles," *Appl. Energy*, vol. 113, pp. 463–476, Jan. 2014.

[11] G. L. Plett, "Recursive approximate weighted total least squares estimation of battery cell total capacity," *J. Power Sources*, vol. 196, pp. 2319–2331, Feb. 2011.

[12] G. Dong, Z. Chen, J. Wei, C. Zhang, and P. Wang, "An online model-based method for state of energy estimation of lithium-ion batteries using dual filters," *J. Power Sources*, vol. 301, pp. 277–286, Jan. 2016.

[13] G. L. Plett, "Extended Kalman filtering for battery management systems of LiPB-based HEV battery packs–Part 3. State and parameter estimation," *J. Power Sources*, vol. 134, pp. 277–292, Aug. 2004.

[14] J. Kim, S. Lee, and B. H. Cho, "Complementary cooperation algorithm based on DEKF combined with pattern recognition for SOC/capacity estimation and SOH prediction," *IEEE Trans. Power Electron.*, vol. 27, no. 1, pp. 436–451, Jan. 2012.

[15] V.-H. Duong, H. A. Bastawrous, K. Lim, K. W. See, P. Zhang, and S. X. Dou, "Online state of charge and model parameters estimation of the $LiFePO_4$ battery in electric vehicles using multiple adaptive forgetting factors recursive least-squares," *J. Power Sources*, vol. 296, pp. 215–224, Nov. 2015.

[16] Y. He, X. Liu, C. Zhang, and Z. Chen, "A new model for State-of-Charge (SOC) estimation for high-power Li-ion batteries," *Appl. Energy*, vol. 101, pp. 808–814, 2013.

[17] F. Yang, Y. Xing, D. Wang, and K.-L. Tsui, "A comparative study of three model-based algorithms for estimating state-of-charge of lithium-ion batteries under a new combined dynamic loading profile," *Appl. Energy*, vol. 164, pp. 387–399, Feb. 2016.

[18] W. Waag, C. Fleischer, and D. U. Sauer, "Critical review of the methods for monitoring of lithium-ion batteries in electric and hybrid vehicles," *J. Power Sources*, vol. 258, pp. 321–339, Jul. 2014.

[19] J. N. Shen, Y. J. He, Z. F. Ma, H. B. Luo, and Z. F. Zhang, "Online state of charge estimation of lithium-ion batteries: A moving horizon estimation approach," *Chem. Eng. Sci.*, vol. 154, pp. 42–53, Nov. 2016.

[20] N. Lotfi, R. G. Landers, J. Li, and J. Park, "Reduced-order electrochemical model-based soc observer with output model uncertainty estimation," *IEEE Trans. Control Syst. Technol.*, vol. 25, no. 4, pp. 1217–1230, Jul. 2017.

[21] M. Guo, G. Sikha, and R. E. White, "Single-particle model for a lithium-ion cell: Thermal behavior," *J. Electrochem. Soc.*, vol. 158, pp. A122–A132, Dec. 2011.

[22] X. Hu, S. Li, and H. Peng, "A comparative study of equivalent circuit models for Li-ion batteries," *J. Power Sources*, vol. 198, pp. 359–367, Jan. 2012.

[23] J. Reuter, E. Mank, H. Aschemann, and A. Rauh, "Battery state observation and condition monitoring using online minimization," in *Proc. 21st Int. Conf. Methods Models Automat. Robot.*, 2016, pp. 1223–1228.

[24] M. Cacciato, G. Nobile, G. Scarcella, and G. Scelba, "Real-time model-based estimation of SOC and SOH for energy storage systems," *IEEE Trans. Power Electron.*, vol. 32, no. 1, pp. 794–803, Feb. 2017.

[25] H. T. Lin, T. J. Liang, and S. M. Chen, "Estimation of battery state of health using probabilistic neural network," *IEEE Trans. Ind. Informat.*, vol. 9, no. 2, pp. 679–685, May 2013.

[26] J. N. Shen, Y. J. He, and Z. F. Ma, "Simultaneous model selection and parameter estimation for lithium-ion batteries: A sequential MINLP solution approach," *AIChE J.*, vol. 62, pp. 78–89, Sep. 2016.

[27] Y. J. He, J. N. Shen, J. F. Shen, and Z. F. Ma, "State of health estimation of lithium-ion batteries: A multiscale Gaussian process regression modeling approach," *AIChE J.*, vol. 61, pp. 1589–1600, May 2015.

[28] C. V. Rao, J. B. Rawlings, and J. H. Lee, "Constrained linear state estimation—a moving horizon approach," *Automatica*, vol. 37, pp. 1619–1628, Oct. 2001.

[29] E. L. Haseltine and J. B. Rawlings, "Critical evaluation of extended Kalman filtering and moving-horizon estimation," *Ind. Eng. Chem. Res.*, vol. 44, pp. 2451–2460, Jun. 2005.

[30] V. M. Zavala, C. D. Laird, and L. T. Biegler, "A fast moving horizon estimation algorithm based on nonlinear programming sensitivity," *J. Process. Control*, vol. 18, pp. 876–884, Oct. 2008.

[31] R. López-Negrete, S. C. Patwardhan, and L. T. Biegler, "Constrained particle filter approach to approximate the arrival cost in Moving Horizon Estimation," *J. Process. Control*, vol. 21, pp. 909–919, Jul. 2011.
[32] C. V. Rao, J. B. Rawlings, and D. Q. Mayne, "Constrained state estimation for nonlinear discrete-time systems: stability and moving horizon approximations," *IEEE Trans. Autom. Control*, vol. 48, no. 2, pp. 246–258, Feb. 2003.

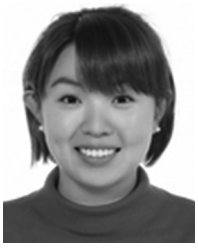

Jia-Ni Shen received the B.Sc. degree from Shanghai Jiao Tong University, Shanghai, China, in 2006, the M.Sc. degree from the Dalian Institute of Chemical Physics, Chinese Academy of Sciences, Dalian, China, in 2009, and the Ph.D. degree from Shanghai Jiao Tong University, in 2017, all in chemical engineering.

She is currently an Assistant Professor with the Department of Chemical Engineering, Shanghai Jiao Tong University. Her research interests include modeling, optimization, and monitoring of energy storage systems.

Jia-Jin Shen is currently working toward the bachelor degree in statistics at the School of Statistics, East China Normal University, Shanghai, China.

Her research interests include mathematical statistics and monitoring of energy storage systems.

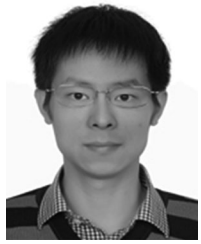

Yi-Jun He received the B.Sc. and Ph.D. degrees in chemical engineering from Zhejiang University, Hangzhou, China, in 2003 and 2008, respectively.

He is currently an Associate Professor with the Department of Chemical Engineering, Shanghai Jiao Tong University, Shanghai, China. He was a Postdoctoral Researcher with the Department of Chemical Engineering, Zhejiang University, between 2008–2010. He was also a Visiting Scholar with the Department of Chemical Engineering, Carnegie Mellon University, Pittsburgh, PA, USA, between 2013 and 2014. His research interests include modeling, optimization, and control of complex industrial systems.

Zi-Feng Ma received the B.Sc. and M.Sc. degrees in chemical engineering from Zhejiang University, Hangzhou, China, in 1985 and 1988, respectively, and the Ph.D. degree in chemical engineering from the South China University of Technology, Guangzhou, China, in 1995.

He is currently a Distinguished Professor with the Department of Chemical Engineering, Shanghai Jiao Tong University and the Founding Director of the Shanghai Electrochemical Energy Devices Research Centre, Shanghai, China. He was the Chair of the Department of Chemical Engineering, Shanghai Jiao Tong University, from 1999 to 2011. He was appointed to be the Chief Scientist of the National Basic Research Program of China for electrochemical energy system in 2007 and 2013, respectively. His research interests include development of advanced energy materials and electrochemical energy systems for electric vehicle and energy storage applications.